RESEARCH ARTICLE

New mechanics of traumatic brain injury

Vladimir G. Ivancevic

Abstract The prediction and prevention of traumatic brain injury is a very important aspect of preventive medical science. This paper proposes a new *coupled loading-rate hypothesis* for the traumatic brain injury (TBI), which states that the main cause of the TBI is an *external Euclidean jolt*, or *SE*(3)-jolt, an impulsive loading that strikes the head in several coupled degrees-of-freedom simultaneously. To show this, based on the previously defined *covariant force law*, we formulate the coupled Newton–Euler dynamics of brain's micro-motions within the cerebrospinal fluid and derive from it the coupled *SE*(3)-jolt dynamics. The *SE*(3)-jolt is a cause of the TBI in two forms of brain's rapid discontinuous deformations: translational dislocations and rotational disclinations. Brain's *dislocations and disclinations*, caused by the *SE*(3)-jolt, are described using the Cosserat multipolar viscoelastic continuum brain model.

Keywords Traumatic brain injuries ·
Coupled loading-rate hypothesis · Euclidean jolt ·
Coupled Newton–Euler dynamics ·
Brain's dislocations and disclinations

Introduction

Traumatic brain injury (TBI) continues to be a major health problem, with over 500,000 cases per year with a societal cost of approximately $85 billion in the US. Motor vehicle accidents are the leading cause of such injuries. In many cases of TBI widespread disruption of the axons occurs through a process known as diffuse axonal injury (DAI) or traumatic axonal injury (TAI) (Singh et al. 2006). TBI occurs when physical trauma causes brain damage, which can result from a closed head injury[1] or a penetrating head injury.[2] In both cases, TBI is caused by rapid deformation of the brain, resulting in a cascade of pathological events and ultimately neuro-degeneration. Understanding how the biomechanics of brain deformation leads to tissue damage remains a considerable challenge (Morrison et al. 2006).

Parts of the brain that can be damaged include the cerebral hemispheres, cerebellum, and brain stem. TBI can cause a host of physical, cognitive, emotional, and social effects (NIH 2002; Rapp 2008). Half of all TBIs are due to transportation accidents involving automobiles, motorcycles, bicycles, and pedestrians. These accidents are the major cause of TBI in people under age 75. For those aged 75 and older, falls cause the majority of TBIs. Approximately 20% of TBIs are due to violence, such as firearm assaults and child abuse, and about 3% are due to sports injuries. Fully half of TBI incidents involve alcohol use (NIH 2002). TBI is a frequent cause of major long-term disability in individuals surviving head injuries sustained in war zones. This is becoming an issue of growing concern in modern warfare in which rapid deployment of acute interventions are effective in saving the lives of combatants with significant head injuries. Traumatic brain injury has been identified as the 'signature injury' among wounded soldiers of the current military engagement in Iraq (Mason 2007; Hoge 2008). Rapid deformation of brain matter caused by skull acceleration is most likely the cause of

V. G. Ivancevic (✉)
Land Operations Division, Defence Science & Technology
Organisation, Adelaide, SA, Australia
e-mail: Vladimir.Ivancevic@dsto.defence.gov.au

---

[1] A closed injury occurs when the head suddenly and violently hits an object but the object does not break through the skull.

[2] A penetrating injury occurs when an object pierces the skull and enters brain tissue.

concussion, as well as more severe TBI. The inability to measure deformation directly has led to disagreement and confusion about the biomechanics of concussion and TBI (Bayly et al. 2005).

TBI can be mild, moderate, or severe, depending on the extent of the damage to the brain. Outcome can be anything from complete recovery to permanent disability or death (see Chen et al. 2008). Some symptoms are evident immediately, while others do not surface until several days or weeks after the injury (NIH 2002). With mild TBI, the patient may remain conscious or may lose consciousness for a few seconds or minutes; the person may also feel dazed or not like him- or herself for several days or weeks after the initial injury; other symptoms include: headache, mental confusion, lightheadedness, dizziness, double vision, blurred vision (or tired eyes), ringing in the ears, bad taste in the mouth, fatigue or lethargy, a change in sleep patterns, behavioral or mood changes, trouble with memory/concentration/calculation. With moderate or severe TBI, the patient may show these same symptoms, but may also have: loss of consciousness, personality change, a severe/persistent/worsening headache, repeated vomiting/nausea, seizures, inability to awaken, dilation (widening) of one or both pupils, slurred speech, weakness/ numbness in the extremities, loss of coordination, increased confusion, restlessness/agitation; vomiting and neurological deficit together are important indicators of prognosis and their presence may warrant early CT scanning and neurosurgical intervention.

In particular, standard medical statistics suggest that the loss of consciousness in boxing knock-outs and road-vehicle crashes is caused by *rotation of the brain-stem* (Misra and Chakravarty 1984) as a dynamic response

(Ivancevic and Ivancevic 2006a; Ivancevic 2007d) of a head–neck system to an impulsive load (Misra and Chakravarty 1985). It is generally associated to the following three syndromes: *Locked-In*, *Semi-Coma*, and *Akinetic Mute*, all three characterized by the total loss of gesture, speech and movement. The cognitive abilities (Ivancevic and Ivancevic 2007c; Ivancevic and Aidman 2007) can still be intact, but the patient cannot express himself by either speech or gesture. Recall that the brain stem, including Midbrain, Pons and Medulla Oblongata, is located at the base of the brain. It is the connection between the cortex and the spinal cord, containing motor neural pathways for voluntary movement from the upper part of the brain. The brain stem also controls such automatic functions as breathing, heart rate, blood pressure, swallowing, sleep patterns and body temperature. Weaker injuries include another three symptoms: *abnormal respiration* (hyperventilation and abnormal breathing patterns: ataxic, clustered, hiccups); *pupils*: dilated, fixed; and *movement* (if any): abnormal extensor.

The natural cushion that protects the brain from trauma is the *cerebrospinal fluid* (CSF). It resides within cranial and spinal cavities and moves in a pulsatile fashion to and from the cranial cavity (see Fig. 1). This motion can be measured by functional magnetic resonance imaging (fMRI, see Sokoloff 2008 for a review) and may be of clinical importance in the diagnosis of several brain and spinal cord disorders such as hydrocephalus, Chiari malformation, and syringomyelia. It was found in (Maier et al. 1994) that brain and CSF of healthy volunteers exhibited periodic motion in the frequency range of normal heart rate. Both brain hemispheres showed periodic squeezing of the ventricles, with peak velocities up to 1 mm/s followed by a slower recoil.

Fig. 1 Human brain and its SE(3)-group of microscopic three-dimensional (3D) motions within the cerebrospinal fluid inside the cranial cavity
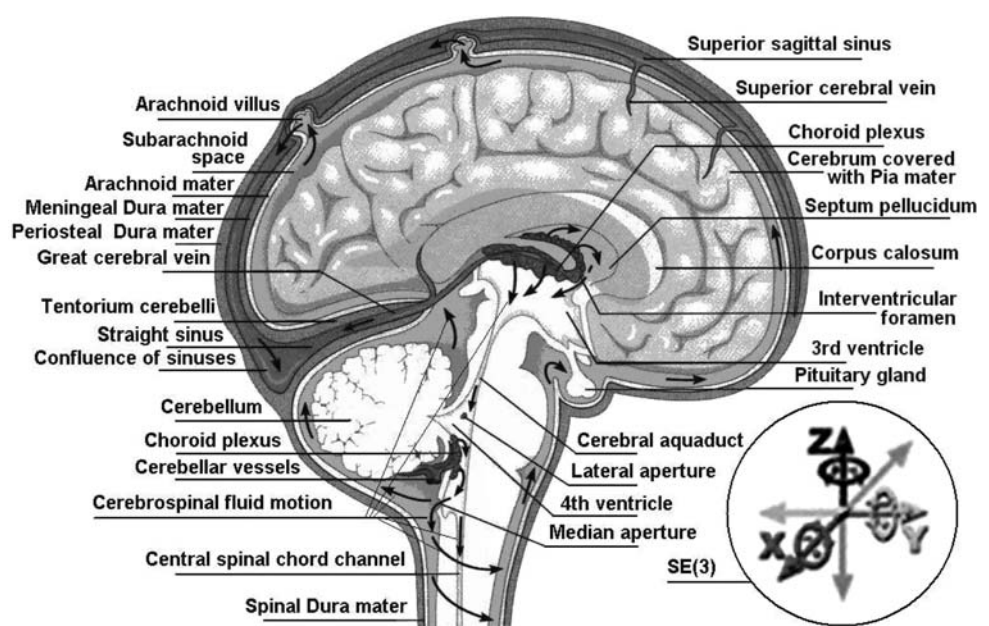
Superimposed on the regular displacement of the brain stem was a slow, respiratory-related periodic shift of the neutral position. During the Valsalva maneuver, the brain stem showed initial caudal and subsequent cranial displacement of 2–3 mm. Coughing produced a short swing of CSF in the cephalic direction. The pressure gradient waveform of a linearized Navier-Stokes model of the pulsatile CSF flow was found in (Loth et al. 2001) to be almost exclusively dependent on the flow waveform and cross-sectional area.

The state of head injury biomechanics: past, present, and future was presented in (Goldsmith 2001), dealing with components and geometry of the human head, classification of head injuries, tolerance considerations, head motion and load characterization, experimental dynamic loading of human living and cadaver heads, dynamic loading of surrogate heads, and head injury mechanics. The subsequent paper (Goldsmith and Monson 2005) described physical head injury experimentation involving animals (primarily primates), human cadavers, volunteers, and inanimate physical models.

Besides motor accidents, concussion (or mild TBI), occurs in many activities, mostly as a result of the head being accelerated. For example, although a popular endeavor, boxing has fallen under increased scrutiny because of its association with TBI. The injury rate in professional boxing matches is high, particularly among male boxers. Superficial facial lacerations are the most common injury reported. Male boxers have a higher rate of knockout and technical knockouts than female boxers (Bledsoe et al. 2005). Although the epidemiology and mechanics of concussion in sports have been investigated for many years, the biomechanical factors that contribute to mild TBI remain unclear because of the difficulties in measuring impact events in the field. The objective of (Beckwith et al. 2007) was to validate an instrumented boxing headgear (IBH) that can be used to measure impact severity and location during play. Based on this study, the IBH is a valid system for measuring head acceleration and impact location that can be integrated into training and competition. Similarly, a comprehensive study has been conducted by Newman et al. (2005) to understand better the mechanics of the impacts associated with concussion in American football, involving a sequence of techniques to analyze and reconstruct many different head impact scenarios.

Impact biomechanics from boxing punches causing translational and rotational head acceleration was experimentally studied in Viano et al. (2005). Olympic boxers threw four different punches at an instrumented Hybrid III dummy and responses were compared with laboratory-reconstructed NFL concussions. Instrumentation included translational and rotational head acceleration and neck loads in the dummy. Biaxial acceleration was measured in the boxer's hand to determine punch force. Hybrid III dummy head responses and FE brain modelling were compared to similarly determined responses from reconstructed concussions in professional NFL football players. The hook produced the highest change in hand velocity (11.0 ± 3.4 m/s) and greatest punch force (4405 ± 2318 N) with average neck load of 855 ± 537 N. It caused head translational and rotational accelerations of 71.2 ± 32.2 g and 9306 ± 4485 r/s^2. These levels are consistent with those causing concussion in NFL impacts. However, the head injury criterion (HIC) for boxing punches was lower than for NFL concussions because of shorter duration acceleration. Boxers deliver punches with proportionally more rotational than translational acceleration than in football concussion. Boxing punches have a 65 mm effective radius from the head cg, which is almost double the 34 mm in football. A smaller radius in football prevents the helmets from sliding off each other in a tackle. Similarly, impacts causing concussion in professional football were simulated in laboratory tests to determine collision mechanics (Viano et al. 2007). This study focused on the biomechanics of concussion in the struck player, addressing head responses causing concussion in the NFL players.

Head injury mechanisms are difficult to study experimentally due to the variety of impact conditions involved, as well as ethical issues, such as the use of human cadavers and animals (Krabbel and Appel 1995). A number of finite element (FE) models and analysis studies have been conducted in order to understand the mechanism of TBI. An FE analysis was carried out in (Chu et al. 1994) to study the mechanism of cerebral contusion. Clinical findings indicate that most cerebral contusions in the absence of skull fracture occur at the frontal and temporal lobes. To explain these observations, cavitation and shear strain theories have long been advocated. Plane strain finite element models of a parasagittal section of the human head were developed in the present study. The model was first validated against a set of experimental results from the literature. Frontal and occipital impacts were then simulated, and pressure and shear stress distributions in the brain were compared. While comparable negative pressures always developed in the contrecoup regions, shear stress distributions remained nearly identical regardless of the impact direction, consistent with the clinically observed pattern for contusion. Therefore, shear strain theory appeared to account better for the clinical findings in cerebral contusion.

A 3D FE model based on the anatomical features of the adult human cranium was developed in Krabbel and Appel (1995). The complex cranial geometry was measured from a series of 2D computer tomography images. The CT scans were transformed with a self-developed preprocessor into a finite element mesh. A review of the existing FE models

was presented in Voo et al. (1996) for the biomechanics of human head injury. More recent models incorporated anatomic details with higher precision. The cervical vertebral column and spinal cord were included. Model results had been more qualitative than quantitative owing to the lack of adequate experimental validation. Advances included transient stress distribution in the brain tissue, frequency responses, effects of boundary conditions, pressure release mechanism of the foramen magnum and the spinal cord, verification of rotation and cavitation theories of brain injury, and protective effects of helmets. These theoretical results provided a basic understanding of the internal biomechanical responses of the head under various dynamic loading conditions. The mechanism of brain contusion has been investigated in Huang et al. (2000) using a series of 3D FE analyses. A head injury model was used to simulate forward and backward rotation around the upper cervical vertebra. Intracranial pressure and shear stress responses were calculated and compared. The results obtained with this model support the predictions of cavitation theory that a pressure gradient develops in the brain during indirect impact. Contrecoup pressure–time histories in the para-sagittal plane demonstrated that an indirect impact induced a smaller intracranial pressure (-53.7 kPa for backward rotation, and -65.5 kPa for forward rotation) than that caused by a direct impact. Comparison of brain responses between frontal and lateral impacts was performed in Zhang et al. (2001) by FE modelling. Identical impact and boundary conditions were used for both the frontal and lateral impact simulations. Intracranial pressure and localized shear stress distributions predicted from these impacts were analyzed. The model predicted higher positive pressures accompanied by a relatively large localized skull deformation at the impact site from a lateral impact when compared to a frontal impact. Lateral impact also induced higher localized shear stress in the core regions of the brain.

A nonlinear viscoelastic FE model for brain tissue was developed in Brands et al. (2004). To obtain sufficient numerical accuracy for modelling the nearly incompressible brain tissue, deviatoric and volumetric stress contributions were separated. Deviatoric stress was modelled in a nonlinear viscoelastic differential form. An attempt was made in Zhang et al. (2004) to delineate actual injury causation and establish a meaningful injury criterion through the use of the actual field accident data. Twenty-four head-to-head field collisions that occurred in professional football games were duplicated using a validated FE human head model. The injury predictors and injury levels were analyzed based on resulting brain tissue responses and were correlated with the site and occurrence of mild TBI. Predictions indicated that the shear stress around the brainstem region could be an injury predictor for concussion. The controlled cortical

impact model has been used extensively to study focal traumatic brain injury. Although the impact variables can be well defined, little is known about the biomechanical trauma as delivered to different brain regions. The FE analysis based on high resolution T2-weighted MRI images of rat brain was used in Pena et al. (2005) to simulate displacement, mean stress, and shear stress of brain during impact. Young's Modulus E, to describe tissue elasticity, was assigned to each FE in three scenarios: in a constant fashion ($E = 50$ kPa), or according to the MRI intensity in a linear ($E = [10, 100]$ kPa) and inverse-linear fashion ($E = [100, 10]$ kPa). Simulated tissue displacement did not vary between the three scenarios, however mean stress and shear stress were largely different. The linear scenario showed the most likely distribution of stresses.

A detailed FE model of the rat brain was developed in Mao et al. (2006) for the prediction of intracranial responses due to different impact scenarios. The FE model was used to predict biomechanical responses within the brain due to controlled cortical impacts (CCI). A total of six different series of CCI studies, four with unilateral craniotomy and two with bilateral craniotomy, were simulated and the results were systematically analyzed, including strain, strain rate and pressure within the rat brain. Simulation results indicated that intracranial strains best correlated with experimentally obtained injuries. An automating meshing method for patient-specific FE model was developed in Guan et al. (2006). 3D geometries of two 6-month-old infant heads were reconstructed from the CT data. FE meshes including cranial bone of skull, brain, and suture were generated. Both static and dynamic analyzes were performed to verify the models. The study for blunt impact of infant head was performed by using these patient-specific models.

A 3D FE analysis of human head was performed in Zong et al. (2006), to assess injury likelihood of the head subjected to impact loading. The structural intensity (SI) methodology[3] was introduced in accordance with the prevailing practice in experimental biomechanics. The SI field inside the head model was computed for three frontal, rear and side impacts. The results for the three cases revealed that there existed power flow paths. The skull was, in general, a good energy flow channel. This study also revealed the high possibility of spinal cord injury due to wave motion inside the head. Recently, a 3D FE analysis was performed in Takahashi et al. (2007) in respect to the frequency analysis of the pressure changes related to TBI. From the results of computer simulations and impact experiments, the authors found similar spectrums in some frequency bands, which indicated the occurrence of the brain injury. A vigorous shaking and an inflicted impact

---

[3] SI is a vector quantity indicating the direction and magnitude of power flow inside a dynamically loaded structure.

were compared in Roth et al. (2007), defined as the terminal portion of a vigorous shaking, using a FE model of a 6-month-old child head. Whereas the calculated values in terms of shearing stress and brain pressure remain different and corroborate the previous studies based on angular and linear velocity and acceleration, the calculated relative brain and skull motions that can be considered at the origin of a subdural haematoma show similar results for the two simulated events. A 2D FE model was developed in Li et al. (2007) with objective to determine localized brain's strains in lateral impact using finite element modelling and evaluate the role of the falx. Motions and strains from the stress analysis matched well with experimental results from literature. A parametric study was conducted by introducing flexible falx in the finite element model. For the model with the rigid falx, high strains were concentrated in the corpus callosum, whereas for the model with the flexible falx, high strains extended into the cerebral vertex.

On the other hand, it has been a common perception that *rapid head rotation* is a major cause of brain damage in automobile crashes and falls. A model for *rotational acceleration* about the center of mass of the rabbit head was presented in Gutierrez et al. (2001), which allowed the study of brain injury without translational acceleration of the head. In the companion paper (Runnerstam et al. 2001) it was shown that rotational head acceleration caused extensive subarachnoid hemorrhage, focal tissue bleeding, reactive astrocytosis, and axonal damage. The initial response of the brain after rotational head injury involved brain edema after 24 h and an excitotoxic neuronal micro-environment in the first hour, which leaded to extensive delayed neuronal cell death by apoptosis necrosis in the cerebral cortex, hippocampus and cerebellum. Similarly, the study by Zhang et al. (2006) used the SIMon human FE head model and delineated the contributions of these accelerations using post mortem human subject (PMHS) lateral head impact experimental data. Results indicated that rotational acceleration contributed more than 90% of total strain, and translational acceleration produced minimal strain.

The fidelity of cell culture TBI—simulations that yield tolerance and mechanistic information relies on both the cellular models and mechanical insult parameters. An electro-mechanical cell shearing device was designed by LaPlaca et al. (2005) in order to produce a controlled high strain rate injury (up to 0.50 strain, 30 s(−1) strain rate) that deforms 3D neural cultures (neurons or astrocytes in an extracellular matrix scaffold). Theoretical analysis revealed that these parameters generated a heterogeneous 3D strain field throughout the cultures that was dependent on initial cell orientation within the matrix, resulting in various combinations of normal and shear strain.

Rigid-body modelling (RBM) was used in Wolfson et al. (2005) to investigate the effect of neck stiffness on head motion and head-torso impacts as a possible mechanism of injury. Realistic shaking data obtained from an anthropometric test dummy (ATD) was used to simulate shaking. In each study injury levels for concussion were exceeded, though impact-type characteristics were required to do so in the neck stiffness study. Levels for the type of injury associated with the syndrome were not exceeded.

The nonlinear mechanical behavior of porcine brain tissue in large shear deformations was determined in Hrapko et al. (2006). An improved method for rotational shear experiments was used, producing an approximately homogeneous strain field and leading to an enhanced accuracy. The model was formulated in terms of a large strain viscoelastic framework and considers nonlinear viscous deformations in combination with non-linear elastic behavior.

The relative motion of the brain with respect to the skull has been widely studied to investigate brain injury mechanisms under impacts, but the motion patterns are not yet thoroughly understood. The study of Zou et al. (2007) analyzed brain motion patterns using the most recent and advanced experimental relative brain/skull motion data collected under low-severity impacts. With a minimum total pseudo-strain energy, the closed-form solutions for rigid body translation and rotation were obtained by matching measured neutral density target (NDT) positions with initial NDT positions. The brain motion was thus separated into rigid body displacement and deformation. The results showed that the brain had nearly pure rigid body displacement at low impact speed. As the impact became more severe, the increased brain motion primarily was due to deformation, while the rigid body displacement was limited in magnitude for both translation and rotation. Under low-severity impacts in the sagittal plane, the rigid body brain translation had a magnitude of 4–5 mm, and the whole brain rotation was on the order of $\pm5°$.

Biomechanical studies using postmortem human subjects (PMHS) in lateral impact have focused primarily on chest and pelvis injuries, mechanisms, tolerances, and comparison with side impact dummies. The objective of (Yoganandan et al. 2008) was to determine lateral impact-induced 3D temporal forces and moments at the head–neck junction and cranial linear and angular accelerations from sled tests using PMHS and compare with responses obtained from an anthropomorphic test device (dummy) designed for lateral impact. Results indicated that profiles of forces and moments at the head–neck junction and cranial accelerations were similar between the two models. However, peak forces and moments at the head–neck junction, as well as peak cranial linear and angular accelerations, were lower in the dummy than PMHS. Peak cranial angular accelerations were suggestive of mild TBI with potential for loss of consciousness.

Deformation of the human brain was measured in vivo by Sabet et al. (2008) in tagged magnetic resonance images (MRI) obtained dynamically during angular acceleration of the head, in order to provide quantitative experimental data to illuminate the mechanics of TBI. Mild angular acceleration was imparted to the skull of a human volunteer inside an MR scanner, using a custom MR-compatible device to constrain motion. Deformation of the brain was characterized quantitatively via Lagrangian strain. Consistent patterns of radial-circumferential shear strain occurred in the brain, similar to those observed in models of a viscoelastic gel cylinder subjected to angular acceleration. It has been noted, however, that strain fields in the brain are clearly mediated by the effects of heterogeneity, divisions between regions of the brain (such as the central fissure and central sulcus) and brain's tethering and suspension system, including the dura mater, falx cerebri, and tentorium membranes.

The present paper proposes a new approach to brain injury dynamics, phrased as a *coupled loading–rate hypothesis* for TBI, stating that the main cause of TBI is an *external Euclidean jolt*, symbolically an *SE*(3)-jolt, an impulsive loading striking the head in several degrees-of-freedom (both translational and rotational) *combined*. This new concept is radically different from any of the standard FEM techniques proposed so far for brain injury mechanics (see the above literature review), as well as from any kind of Newton–Eulerian or Lagrangian/Hamiltonian injury dynamics, emphasizing three new aspects of brain injury mechanics: (i) coupling of all 6 degrees-of-freedom; (ii) jolt dynamics rather than the force dynamics; and (iii) coupled dislocations/disclinations in the Cosserat multipolar viscoelastic continuum brain model. This new concept is a derivation of our previously defined concept of the *covariant force law* (Ivancevic and Ivancevic 2006b, c, 2007e, 2008). To support this hypothesis, we develop the coupled Newton–Euler dynamics of the brains's micro-motions within the cerebrospinal fluid (see Fig. 1), and from it derive the *SE*(3)-jolt dynamics, as well as its biophysical consequences in the form of brain's dislocations and disclinations.

The *SE*(3)-jolt: the cause of TBI

In the language of modern dynamics (Ivancevic and Ivancevic 2006b, c, 2007d, e), the microscopic motion of human brain within the skull is governed by the Euclidean *SE*(3)-group of 3D motions (see next subsection). Within the brain's *SE*(3)-group we have both *SE*(3)-kinematics (consisting of *SE*(3)-velocity and its two time derivatives: *SE*(3)-acceleration and *SE*(3)-jerk) and *SE*(3)-dynamics (consisting of *SE*(3)-momentum and its two time derivatives: *SE*(3)-force and *SE*(3)-jolt), which defines brain's kinematics × brain's mass-inertia distribution.

Informally, the external *SE*(3)-jolt[4] is a sharp and sudden change in the *SE*(3)-force acting on brain's mass–inertia distribution (given by brain's mass and inertia matrices). That is, a 'delta'-change in a 3D force–vector coupled to a 3D torque–vector, striking the head-shell with the brain immersed into the cerebrospinal fluid. In other words, the *SE*(3)-jolt is a sudden, sharp and discontinues shock in all six coupled dimensions of brain's continuous micro-motion within the cerebrospinal fluid (Fig. 1), namely within the three Cartesian (*x*, *y*, *z*)-translations and the three corresponding Euler angles around the Cartesian axes: roll, pitch and yaw. If the *SE*(3)-jolt produces a mild shock to the brain (e.g., strong head shake), it causes mild TBI, with temporary disabled associated sensory-motor and/or cognitive functions and affecting respiration and movement. If the *SE*(3)-jolt produces a hard shock (hitting the head with external mass), it causes severe TBI, with the total loss of gesture, speech and movement.

The *SE*(3)-jolt is rigorously defined in terms of differential geometry (Ivancevic and Ivancevic 2006c, 2007c, e). Briefly, it is the absolute time-derivative of the covariant force 1-form (or, co-vector field). The fundamental law of biomechanics is the *covariant force law* (Ivancevic and Ivancevic 2006b, c, 2007e), which states:

Force co-vector field = Mass distribution
$$\times \text{ Acceleration vector-field,}$$

which is formally written (using the Einstein summation convention, with indices labelling the three Cartesian translations and the three corresponding Euler angles):

$$F_\mu = m_{\mu v} a^v, \quad (\mu, v = 1, \ldots, 6)$$

where F_μ denotes the six covariant components of the external "pushing" *SE*(3)-force co-vector field, $m_{\mu v}$ represents the 6×6 covariant components of brain's inertia–metric tensor, while a^v corresponds to the six contravariant components of brain's internal *SE*(3)-acceleration vector-field.

Now, the covariant (absolute, Bianchi) time-derivative $\frac{\mathrm{D}}{\mathrm{d}t}(\cdot)$ of the covariant *SE*(3)-force F_μ defines the corresponding external "striking" *SE*(3)-jolt co-vector field:

$$\frac{\mathrm{D}}{\mathrm{d}t}(F_\mu) = m_{\mu v}\frac{\mathrm{D}}{\mathrm{d}t}(a^v) = m_{\mu v}\left(\dot{a}^v + \Gamma^v_{\mu\lambda}a^\mu a^\lambda\right), \tag{1}$$

---

[4] The mechanical *SE*(3)-jolt concept is based on the mathematical concept of higher-order tangency (rigorously defined in terms of jet bundles of the head's configuration manifold) (Ivancevic and Ivancevic 2006c, e), as follows: When something hits the human head, or the head hits some external body, we have a collision. This is naturally described by the *SE*(3)-momentum, which is a nonlinear coupling of three linear Newtonian momenta with three angular Eulerian momenta. The tangent to the *SE*(3)-momentum, defined by the (absolute) time derivative, is the *SE*(3)-force. The second-order tangency is given by the *SE*(3)-jolt, which is the tangent to the *SE*(3)-force, also defined by the time derivative.

where $\frac{D}{dt}(a^\nu)$ denotes the six contravariant components of the brain's internal SE(3)-jerk vector-field and overdot (˙) denotes the time derivative. $\Gamma^\nu_{\mu\lambda}$ are the Christoffel's symbols of the Levi–Civita connection for the brain's SE(3)-group, which are zero in case of pure Cartesian translations and nonzero in case of rotations as well as in the full-coupling of translations and rotations.

In the following, we elaborate on the SE(3)-jolt concept (using vector and tensor methods) and its biophysical TBI consequences in the form of brain's dislocations and disclinations.

SE(3)-group of brain's micro-motions within the CSF

The brain and the CSF together exhibit periodic microscopic translational and rotational motion in a pulsatile fashion to and from the cranial cavity, in the frequency range of normal heart rate (with associated periodic squeezing of brain's ventricles) (Maier et al. 1994). This micro-motion is mathematically defined by the Euclidean (gauge) SE(3)-group. Briefly, the SE(3)-group is defined as a semidirect (noncommutative) product of 3D rotations and 3D translations,

$$SE(3) := SO(3) \rhd \mathbb{R}^3.$$

Its most important subgroups are the following (see Appendix for technical details):

Subgroup	Definition
SO(3), group of rotations in 3D (a spherical joint)	Set of all proper orthogonal 3 × 3-rotational matrices
SE(2), special Euclidean group in 2D (all planar motions)	Set of all 3 × 3-matrices: $\begin{bmatrix} \cos\theta & \sin\theta & r_x \\ -\sin\theta & \cos\theta & r_y \\ 0 & 0 & 1 \end{bmatrix}$
SO(2), group of rotations in 2D subgroup of SE(2)—group (a revolute joint)	Set of all proper orthogonal 2 × 2-rotational matrices included in SE(2)- group
$\mathbb{R}^3$, group of translations in 3D (all spatial displacements)	Euclidean 3D vector space

In other words, the gauge SE(3)-group of Euclidean micro-motions of the brain immersed in the cerebrospinal fluid within the cranial cavity, contains matrices of the form $\begin{pmatrix} \mathbf{R} & \mathbf{b} \\ 0 & 1 \end{pmatrix}$, where $\mathbf{b}$ is the brain's 3D micro-translation vector and $\mathbf{R}$ is the brain's 3D rotation matrix, given by the product $\mathbf{R} = R_\varphi \cdot R_\psi \cdot R_\theta$ of the brain's three Eulerian micro-rotations, roll = R_φ, pitch = R_ψ, yaw = R_θ, performed respectively about the x-axis by the angle φ, about the y-axis by the angle ψ, and about the z-axis by the angle θ (Ivancevic 2004; Park and Chung 2005; Ivancevic 2006),

$$R_\varphi = \begin{bmatrix} 1 & 0 & 0 \\ 0 & \cos\varphi & -\sin\varphi \\ 0 & \sin\varphi & \cos\varphi \end{bmatrix},$$

$$R_\psi = \begin{bmatrix} \cos\psi & 0 & \sin\psi \\ 0 & 1 & 0 \\ -\sin\psi & 0 & \cos\psi \end{bmatrix},$$

$$R_\theta = \begin{bmatrix} \cos\theta & -\sin\theta & 0 \\ \sin\theta & \cos\theta & 0 \\ 0 & 0 & 1 \end{bmatrix}.$$

Therefore, brain's natural SE(3)-dynamics within the cerebrospinal fluid is given by the coupling of Newtonian (translational) and Eulerian (rotational) equations of micro-motion within the CSF.

Brain's natural SE(3)-dynamics

To support our coupled loading-rate hypothesis, we formulate the coupled Newton–Euler dynamics of brain's micro-motions within the scull's SE(3)-group of motions. The forced Newton–Euler equations read in vector (boldface) form

$$\begin{aligned} \text{Newton}: \dot{\mathbf{p}} \equiv \mathbf{M}\dot{\mathbf{v}} &= F + \mathbf{p} \times \boldsymbol{\omega}, \\ \text{Euler}: \dot{\boldsymbol{\pi}} \equiv \boldsymbol{I}\dot{\boldsymbol{\omega}} &= T + \pi \times \omega + \mathbf{p} \times \mathbf{v}, \end{aligned} \quad (2)$$

where $\times$ denotes the vector cross product,[5]

$$\begin{aligned} \mathbf{M} &\equiv M_{ij} = \text{diag}\{m_1, m_2, m_3\} \quad \text{and} \\ \mathbf{I} &\equiv I_{ij} = \text{diag}\{I_1, I_2, I_3\}, \quad (i,j = 1,2,3) \end{aligned}$$

are brain's (diagonal) mass and inertia matrices,[6] defining brain's mass–inertia distribution, with principal inertia moments given in Cartesian coordinates (x, y, z) by volume integrals

---

[5] Recall that the cross product $\mathbf{u} \times \mathbf{v}$ of two vectors $\mathbf{u}$ and $\mathbf{v}$ equals $\mathbf{u} \times \mathbf{v} = uv \sin\theta\mathbf{n}$, where θ is the angle between $\mathbf{u}$ and $\mathbf{v}$, while $\mathbf{n}$ is a unit vector perpendicular to the plane of $\mathbf{u}$ and $\mathbf{v}$ such that $\mathbf{u}$ and $\mathbf{v}$ form a right-handed system.

[6] In reality, mass and inertia matrices ($\mathbf{M}$, $\mathbf{I}$) are not diagonal but rather full 3 × 3 positive-definite symmetric matrices with coupled mass- and inertia-products. Even more realistic, fully-coupled mass–inertial properties of a brain immersed in (incompressible, irrotational and inviscid) cerebrospinal fluid are defined by the single non-diagonal 6 × 6 positive-definite symmetric mass–inertia matrix $\mathcal{M}_{SE(3)}$, the so-called material metric tensor of the SE(3)-group, which has all nonzero mass–inertia coupling products. In other words, the 6 × 6 matrix $\mathcal{M}_{SE(3)}$ contains: (i) brain's own mass plus the added mass matrix associated with the fluid, (ii) brain's own inertia plus the added inertia matrix associated with the potential flow of the fluid, and (iii) all the coupling terms between linear and angular momenta. However, for simplicity, in this paper we shall consider only the simple case of two separate diagonal 3 × 3 matrices ($\mathbf{M}, \mathbf{I}$).

$$I_1 = \iiint \rho(z^2 + y^2)\mathrm{d}x\mathrm{d}y\mathrm{d}z, \quad I_2 = \iiint \rho(x^2 + z^2)\mathrm{d}x\mathrm{d}y\mathrm{d}z,$$
$$I_3 = \iiint \rho(x^2 + y^2)\mathrm{d}x\mathrm{d}y\mathrm{d}z,$$

dependent on brain's density $\rho = \rho(x, y, z)$,

$$\mathbf{v} \equiv v^i = [v_1, v_2, v_3]^t \quad \text{and} \quad \boldsymbol{\omega} \equiv \omega^i = [\omega_1, \omega_2, \omega_3]^t$$

(where $[\ ]^t$ denotes the vector transpose) are brain's linear and angular velocity vectors[7] (that is, column vectors),

$$\mathbf{F} \equiv F_i = [F_1, F_2, F_3] \quad \text{and} \quad \mathbf{T} \equiv T_i = [T_1, T_2, T_3]$$

are gravitational and other external force and torque co-vectors (that is, row vectors) acting on the brain within the scull,

$$\mathbf{p} \equiv p_i \equiv \mathbf{Mv} = [p_1, p_2, p_3] = [m_1 v_1, m_2 v_2, m_2 v_2] \quad \text{and}$$
$$\boldsymbol{\pi} \equiv \pi_i \equiv \mathbf{I}\boldsymbol{\omega} = [\pi_1, \pi_2, \pi_3] = [I_1 \omega_1, I_2 \omega_2, I_3 \omega_3]$$

are brain's linear and angular momentum co-vectors.

In tensor form, the forced Newton–Euler equations (2) read

$$\dot{p}_i \equiv M_{ij}\dot{v}^j = F_i + \varepsilon_{ik}^j p_j \omega^k, \quad (i, j, k = 1, 2, 3)$$
$$\dot{\pi}_i \equiv I_{ij}\dot{\omega}^j = T_i + \varepsilon_{ik}^j \pi_j \omega^k + \varepsilon_{ik}^j p_j v^k,$$

where the permutation symbol ε_{ik}^j is defined as

$$\varepsilon_{ik}^j = \begin{cases} +1 & \text{if } (i, j, k) \text{ is } (1, 2, 3), (3, 1, 2) \text{ or } (2, 3, 1), \\ -1 & \text{if } (i, j, k) \text{ is } (3, 2, 1), (1, 3, 2) \text{ or } (2, 1, 3), \\ 0 & \text{otherwise}: i = j \text{ or } j = k \text{ or } k = i. \end{cases}$$

In scalar form, the forced Newton–Euler equations (2) expand as

$$\text{Newton}: \begin{cases} \dot{p}_1 = F_1 - m_3 v_3 \omega_2 + m_2 v_2 \omega_3 \\ \dot{p}_2 = F_2 + m_3 v_3 \omega_1 - m_1 v_1 \omega_3, \\ \dot{p}_3 = F_3 - m_2 v_2 \omega_1 + m_1 v_1 \omega_2 \end{cases}$$
$$\text{Euler}: \begin{cases} \dot{\pi}_1 = T_1 + (m_2 - m_3)v_2 v_3 + (I_2 - I_3)\omega_2 \omega_3 \\ \dot{\pi}_2 = T_2 + (m_3 - m_1)v_1 v_3 + (I_3 - I_1)\omega_1 \omega_3, \\ \dot{\pi}_3 = T_3 + (m_1 - m_2)v_1 v_2 + (I_1 - I_2)\omega_1 \omega_2 \end{cases} \quad (3)$$

showing brain's individual mass and inertia couplings.

Equations (2)–(3) can be derived from the translational + rotational kinetic energy of the brain[8]

$$E_k = \frac{1}{2}\mathbf{v}^t\mathbf{Mv} + \frac{1}{2}\boldsymbol{\omega}^t\mathbf{I}\boldsymbol{\omega}, \quad (4)$$

or, in tensor form

---

[7] In reality, $\boldsymbol{\omega}$ is a 3×3 *attitude matrix* (see Appendix). However, for simplicity, we will stick to the (mostly) symmetrical translation-rotation vector form.

[8] In a fully-coupled Newton–Euler brain dynamics, instead of Eq. 4 we would have brain's kinetic energy defined by the inner product:

$$E_k = \frac{1}{2}\begin{bmatrix} \mathbf{p} \\ \boldsymbol{\pi} \end{bmatrix} \mathcal{M}_{SE(3)} \begin{bmatrix} \mathbf{p} \\ \boldsymbol{\pi} \end{bmatrix}.$$

$$E = \frac{1}{2}M_{ij}v^i v^j + \frac{1}{2}I_{ij}\omega^i \omega^j.$$

For this we use the *Kirchhoff–Lagrangian equations* (see, e.g., Lamb 1932; Leonard 1997), or the original work of Kirchhoff written in German)

$$\frac{\mathrm{d}}{\mathrm{d}t}\partial_\mathbf{v}E_k = \partial_\mathbf{v}E_k \times \boldsymbol{\omega} + \mathbf{F},$$
$$\frac{\mathrm{d}}{\mathrm{d}t}\partial_{\boldsymbol{\omega}}E_k = \partial_{\boldsymbol{\omega}}E_k \times \boldsymbol{\omega} + \partial_\mathbf{v}E_k \times \mathbf{v} + \mathbf{T}, \quad (5)$$

where $\partial_\mathbf{v}E_k = \frac{\partial E_k}{\partial \mathbf{v}}, \partial_{\boldsymbol{\omega}}E_k = \frac{\partial E_k}{\partial \boldsymbol{\omega}}$; in tensor form these equations read

$$\frac{\mathrm{d}}{\mathrm{d}t}\partial_{v^i}E = \varepsilon_{ik}^j(\partial_{v^j}E)\omega^k + F_i,$$
$$\frac{\mathrm{d}}{\mathrm{d}t}\partial_{\omega^i}E = \varepsilon_{ik}^j(\partial_{\omega^j}E)\omega^k + \varepsilon_{ik}^j(\partial_{v^j}E)v^k + T_i.$$

Using (4)–(5), brain's linear and angular momentum co-vectors are defined as

$$\mathbf{p} = \partial_\mathbf{v}E_k, \quad \boldsymbol{\pi} = \partial_{\boldsymbol{\omega}}E_k,$$

or, in tensor form

$$p_i = \partial_{v^i}E, \quad \pi_i = \partial_{\omega^i}E,$$

with their corresponding time derivatives, in vector form

$$\dot{\mathbf{p}} = \frac{\mathrm{d}}{\mathrm{d}t}\mathbf{p} = \frac{\mathrm{d}}{\mathrm{d}t}\partial_\mathbf{v}E, \quad \dot{\boldsymbol{\pi}} = \frac{\mathrm{d}}{\mathrm{d}t}\boldsymbol{\pi} = \frac{\mathrm{d}}{\mathrm{d}t}\partial_{\boldsymbol{\omega}}E,$$

or, in tensor form

$$\dot{p}_i = \frac{\mathrm{d}}{\mathrm{d}t}p_i = \frac{\mathrm{d}}{\mathrm{d}t}\partial_{v^i}E, \quad \dot{\pi}_i = \frac{\mathrm{d}}{\mathrm{d}t}\pi_i = \frac{\mathrm{d}}{\mathrm{d}t}\partial_{\omega^i}E,$$

or, in scalar form

$$\dot{\mathbf{p}} = [\dot{p}_1, \dot{p}_2, \dot{p}_3] = [m_1\dot{v}_1, m_2\dot{v}_2, m_3\dot{v}_3],$$
$$\dot{\boldsymbol{\pi}} = [\dot{\pi}_1, \dot{\pi}_2, \dot{\pi}_3] = [I_1\dot{\omega}_1, I_2\dot{\omega}_2, I_3\dot{\omega}_3].$$

While brain's healthy $SE(3)$-dynamics within the cerebrospinal fluid is given by the coupled Newton–Euler micro-dynamics, the TBI is actually caused by the sharp and discontinuous change in this natural $SE(3)$ micro-dynamics, in the form of the $SE(3)$-jolt, causing brain's discontinuous deformations.

Brain's traumatic dynamics: the $SE(3)$-jolt

The $SE(3)$-jolt, the actual cause of the TBI (in the form of the brain's plastic deformations), is defined as a coupled Newton + Euler jolt; in (co)vector form the $SE(3)$-jolt reads[9]

$$SE(3)\text{-jolt}: \begin{cases} \text{Newton jolt}: \dot{\mathbf{F}} = \ddot{\mathbf{p}} - \dot{\mathbf{p}} \times \boldsymbol{\omega} - \mathbf{p} \times \dot{\boldsymbol{\omega}}, \\ \text{Euler jolt}: \dot{\mathbf{T}} = \ddot{\boldsymbol{\pi}} - \dot{\boldsymbol{\pi}} \times \dot{\boldsymbol{\omega}} - \boldsymbol{\pi} \times \dot{\boldsymbol{\omega}} - \dot{\mathbf{p}} \times \mathbf{v} - \mathbf{p} \times \dot{\mathbf{v}}, \end{cases}$$

where the linear and angular jolt co-vectors are

---

[9] Note that the derivative of the cross-product of two vectors follows the standard calculus product-rule: $\frac{\mathrm{d}}{\mathrm{d}t}(\mathbf{u} \times \mathbf{v}) = \dot{\mathbf{u}} \times \mathbf{v} + \mathbf{u} \times \dot{\mathbf{v}}$.

$$\dot{\mathbf{F}} \equiv \mathbf{M}\dddot{\mathbf{v}} = [\dot{F}_1, \dot{F}_2, \dot{F}_3], \quad \dot{\mathbf{T}} \equiv \mathbf{I}\dddot{\boldsymbol{\omega}} = [\dot{T}_1, \dot{T}_2, \dot{T}_3],$$

where

$$\dddot{\mathbf{v}} = [\dddot{v}_1, \dddot{v}_2, \dddot{v}_3]^t, \quad \dddot{\boldsymbol{\omega}} = [\dddot{\omega}_1, \dddot{\omega}_2, \dddot{\omega}_3]^t,$$

are linear and angular jerk vectors.

In tensor form, the $SE(3)$-jolt reads[10]

$$\dot{F}_i = \dddot{p}_i - \varepsilon_{ik}^j \dot{p}_j \omega^k - \varepsilon_{ik}^j p_j \dot{\omega}^k, \quad (i, j, k = 1, 2, 3)$$
$$\dot{T}_i = \dddot{\pi}_i - \varepsilon_{ik}^j \dot{\pi}_j \omega^k - \varepsilon_{ik}^j \pi_j \dot{\omega}^k - \varepsilon_{ik}^j \dot{p}_j v^k - \varepsilon_{ik}^j p_j \dot{v}^k,$$

in which the linear and angular jolt covectors are defined as

$$\dot{\mathbf{F}} \equiv \dot{F}_i = \mathbf{M}\dddot{\mathbf{v}} \equiv M_{ij}\dddot{v}^j = [\dot{F}_1, \dot{F}_2, \dot{F}_3],$$
$$\dot{\mathbf{T}} \equiv \dot{T}_i = \mathbf{I}\dddot{\boldsymbol{\omega}} \equiv I_{ij}\dddot{\omega}^j = [\dot{T}_1, \dot{T}_2, \dot{T}_3],$$

where $\dddot{\mathbf{v}} = \dddot{v}^i$, and $\dddot{\boldsymbol{\omega}} = \dddot{\omega}^i$ are linear and angular jerk vectors.

In scalar form, the $SE(3)$-jolt expands as

$$\text{Newton jolt}: \begin{cases} \dot{F}_1 = \dddot{p}_1 - m_2\omega_3\dot{v}_2 + m_3(\omega_2\dot{v}_3 + v_3\dot{\omega}_2) - m_2 v_2\dot{\omega}_3, \\ \dot{F}_2 = \dddot{p}_2 + m_1\omega_3\dot{v}_1 - m_3\omega_1\dot{v}_3 - m_3 v_3\dot{\omega}_1 + m_1 v_1\dot{\omega}_3, \\ \dot{F}_3 = \dddot{p}_3 - m_1\omega_2\dot{v}_1 + m_2\omega_1\dot{v}_2 - v_2\dot{\omega}_1 - m_1 v_1\dot{\omega}_2, \end{cases}$$

$$\text{Euler jolt}: \begin{cases} \dot{T}_1 = \dddot{\pi}_1 - (m_2 - m_3)(v_3\dot{v}_2 + v_2\dot{v}_3) - (I_2 - I_3)(\omega_3\dot{\omega}_2 + \omega_2\dot{\omega}_3), \\ \dot{T}_2 = \dddot{\pi}_2 + (m_1 - m_3)(v_3\dot{v}_1 + v_1\dot{v}_3) + (I_1 - I_3)(\omega_3\dot{\omega}_1 + \omega_1\dot{\omega}_3), \\ \dot{T}_3 = \dddot{\pi}_3 - (m_1 - m_2)(v_2\dot{v}_1 + v_1\dot{v}_2) - (I_1 - I_2)(\omega_2\dot{\omega}_1 + \omega_1\dot{\omega}_2). \end{cases}$$

We remark here that the linear and angular momenta $(\mathbf{p}, \boldsymbol{\pi})$, forces $(\mathbf{F}, \mathbf{T})$ and jolts $(\dot{\mathbf{F}}, \dot{\mathbf{T}})$ are co-vectors (row vectors), while the linear and angular velocities $(\mathbf{v}, \boldsymbol{\omega})$, accelerations $(\dot{\mathbf{v}}, \dot{\boldsymbol{\omega}})$ and jerks $(\dddot{\mathbf{v}}, \dddot{\boldsymbol{\omega}})$ are vectors (column vectors). This bio-physically means that the 'jerk' vector should not be confused with the 'jolt' co-vector. For example, the 'jerk' means shaking the head's own mass–inertia matrices (mainly in the atlanto–occipital and atlanto–axial joints), while the 'jolt' means actually hitting the head with some external mass–inertia matrices included in the 'hitting' SE(3)-jolt, or hitting some external static/massive body with the head (e.g., the ground—gravitational effect, or the wall—inertial effect). Consequently, the mass-less 'jerk' vector represents a (translational + rotational) *non-collision effect* that can cause only weaker brain injuries, while the inertial 'jolt' co-vector represents a (translational + rotational) *collision effect* that can cause hard brain injuries.

For example, while driving a car, the SE(3)-jerk of the head–neck system happens every time the driver brakes

abruptly. On the other hand, the SE(3)-jolt means actual impact to the head. Similarly, the whiplash–jerk, caused by rear-end car collisions, is like a soft version of the high pitch-jolt caused by the boxing 'upper-cut'. Also, violently shaking the head left–right in the transverse plane is like a soft version of the high yaw-jolt caused by the boxing 'cross-cut'.

Brain's dislocations and disclinations caused by the SE(3)-jolt

Recall from introduction that for mild TBI, the best injury predictor is considered to be the product of brain's strain and strain rate, which is the standard isotropic viscoelastic continuum concept. To improve this standard concept, in this subsection, we consider human brain as a 3D anisotropic multipolar *Cosserat viscoelastic continuum* (Cosserat and Cosserat 1898, 1909; Eringen 2002), exhibiting coupled–stress–strain elastic properties. This non-standard continuum model is suitable for analyzing plastic (irreversible) deformations and fracture mechanics (Bilby and Eshelby 1968) in multi-layered materials with microstructure (in which slips and bending of layers introduces additional degrees of freedom, non-existent in the standard continuum models; see (Mindlin 1965; Lakes 1985) for physical characteristics and (Yang and Lakes 1981, 1982; Park and Lakes 1986) for biomechanical applications).

The $SE(3)$-jolt $(\dot{\mathbf{F}}, \dot{\mathbf{T}})$ causes two types of brain's rapid discontinuous deformations:

(1) The Newton jolt $\dot{\mathbf{F}}$ can cause micro-translational *dislocations*, or discontinuities in the Cosserat translations;
(2) The Euler jolt $\dot{\mathbf{T}}$ can cause micro-rotational *disclinations*, or discontinuities in the Cosserat rotations.

For general treatment on dislocations and disclinations related to asymmetric discontinuous deformations in multipolar materials, see, e.g., (Jian and Xiao-ling 1995; Yang et al. 2001).

To precisely define brain's dislocations and disclinations, caused by the $SE(3)$-jolt $(\dot{\mathbf{F}}, \dot{\mathbf{T}})$, we first define the coordinate

---

[10] In this paragraph the overdots actually denote the absolute Bianchi (covariant) time-derivative (1), so that the jolts retain the proper covector character, which would be lost if ordinary time derivatives are used. However, for the sake of simplicity and wider readability, we stick to the same overdot notation.

co-frame, i.e., the set of basis 1-forms $\{dx^i\}$, given in local coordinates $x^i = (x^1, x^2, x^3) = (x, y, z)$, attached to the brain's center-of-mass. Then, in the coordinate co-frame $\{dx^i\}$ we introduce the following set of brain's plastic-deformation-related $SE(3)$-based differential p-forms[11] (see, e.g., Ivancevic and Ivancevic 2006c, 2007e):

the *dislocation current* 1-form, $\mathbf{J} = J_i\, dx^i$;
the *dislocation density* 2-form, $\boldsymbol{\alpha} = \frac{1}{2}\alpha_{ij}\, dx^i \wedge dx^j$;
the *disclination current* 2-form, $\mathbf{S} = \frac{1}{2}S_{ij}\, dx^i \wedge dx^j$; and
the *disclination density* 3–form,
$\mathbf{Q} = \frac{1}{3!}Q_{ijk}\, dx^i \wedge dx^j \wedge dx^k$,

where $\wedge$ denotes the exterior wedge-product. According to Edelen (1980; Kadic and Edelen 1983), these four $SE(3)-$based differential forms satisfy the following set of continuity equations:

$$\dot{\boldsymbol{\alpha}} = -\mathbf{dJ} - \mathbf{S}, \qquad (6)$$

$$\dot{\mathbf{Q}} = -\mathbf{dS}, \qquad (7)$$

$$\mathbf{d\alpha} = \mathbf{Q}, \qquad (8)$$

$$\mathbf{dQ} = \mathbf{0}, \qquad (9)$$

where $\mathbf{d}$ denotes the exterior derivative.

In components, the simplest, fourth equation (9), representing the so-called *Bianchi identity*, can be rewritten as

$$\mathbf{dQ} = \partial_l Q_{[ijk]}\, dx^l \wedge dx^i \wedge dx^j \wedge dx^k = 0,$$

where $\partial_i \equiv \partial/\partial x^i$, while $\theta_{[ij\ldots]}$ denotes the skew-symmetric part of $\theta_{ij\ldots}$.

---

[11] Differential p-forms are totally skew-symmetric covariant tensors, defined using the exterior wedge-product and exterior derivative. The proper definition of exterior derivative d for a p-form β on a smooth manifold M, includes the *Poincaré lemma* (Ivancevic and Ivancevic 2006c, 2007e): $d(d\beta) = 0$, and validates the *general Stokes formula*

$$\int_{\partial M} \beta = \int_M d\beta,$$

where M is a p-dimensional *manifold with a boundary* and ∂M is its $(p-1)$-dimensional *boundary*, while the integrals have appropriate dimensions.

A p-form β is called *closed* if its exterior derivative is equal to zero,

$$d\beta = 0.$$

From this condition one can see that the closed form (the *kernel* of the exterior derivative operator d) is conserved quantity. Therefore, closed p-forms possess certain invariant properties, physically corresponding to the conservation laws.

A p-form β that is an exterior derivative of some $(p-1)$-form α,

$$\beta = d\alpha,$$

is called *exact* (the *image* of the exterior derivative operator d). By *Poincaré lemma*, exact forms prove to be closed automatically,

$$d\beta = d(d\alpha) = 0.$$

This lemma is the foundation of the de Rham cohomology theory (Ivancevic and Ivancevic 2006c, 2007e).

Similarly, the third equation (8) in components reads

$$\frac{1}{3!}Q_{ijk}\, dx^i \wedge dx^j \wedge dx^k = \partial_k \alpha_{[ij]}\, dx^k \wedge dx^i \wedge dx^j, \quad \text{or}$$
$$Q_{ijk} = -6\partial_k \alpha_{[ij]}.$$

The second equation (7) in components reads

$$\frac{1}{3!}\dot{Q}_{ijk}\, dx^i \wedge dx^j \wedge dx^k = -\partial_k S_{[ij]}\, dx^k \wedge dx^i \wedge dx^j, \quad \text{or}$$
$$\dot{Q}_{ijk} = 6\partial_k S_{[ij]}.$$

Finally, the first equation (6) in components reads

$$\frac{1}{2}\dot{\alpha}_{ij}\, dx^i \wedge dx^j = (\partial_j J_i - \frac{1}{2}S_{ij})\, dx^i \wedge dx^j, \quad \text{or}$$
$$\dot{\alpha}_{ij} = 2\partial_j J_i - S_{ij}.$$

In words, we have:

- The 2-form Eq. (6) defines the time derivative $\boldsymbol{\alpha} \doteq \frac{1}{2}\dot{\alpha}_{ij}\, dx^i \wedge dx^j$ of the dislocation density $\boldsymbol{\alpha}$ as the (negative) sum of the disclination current $\mathbf{S}$ and the curl of the dislocation current $\mathbf{J}$.
- The 3-form Eq. (7) states that the time derivative $\dot{\mathbf{Q}} = \frac{1}{3!}\dot{Q}_{ijk}\, dx^i \wedge dx^j \wedge dx^k$ of the disclination density $\mathbf{Q}$ is the (negative) divergence of the disclination current $\mathbf{S}$.
- The 3-form Eq. (8) defines the disclination density $\mathbf{Q}$ as the divergence of the dislocation density $\boldsymbol{\alpha}$, that is, $\mathbf{Q}$ is the *exact* 3-form.
- The Bianchi identity (9) follows from Eq. 8 by *Poincaré lemma* and states that the disclination density $\mathbf{Q}$ is conserved quantity, that is, $\mathbf{Q}$ is the *closed* 3-form. Also, every 4-form in 3D space is zero.

From these equations, we can derive two important conclusions:

(1) Being the derivatives of the dislocations, brain's disclinations are higher-order tensors, and thus more complex quantities, which means that they present a higher risk for the severe TBI than dislocations—a fact which *is* supported by the literature (see review of existing TBI-models given in Introduction).

(2) Brain's dislocations and disclinations are mutually coupled by the underlaying $SE(3)$-group, which means that we cannot separately analyze translational and rotational TBIs—a fact which *is not* supported by the literature.

Conclusion

Based on the previously developed covariant force law, in this paper we have formulated a new coupled loading-rate hypothesis for the TBI, which states that the main cause of traumatic brain injury is an external $SE(3)$-jolt, an impulsive loading striking the head in several degrees-of-freedom,

both rotational and translational, combined.[12] To demonstrate this, we have developed the vector and tensor Newton–Euler mechanics on the Euclidean $SE(3)$-group of brain's micro-motions within the cerebrospinal fluid. In this way, we have precisely defined the concept of the $SE(3)$-jolt, which is a cause of brain's rapid discontinuous deformations: (i) translational dislocations, and (ii) rotational disclinations. Based on the presented model, we argue that: (1) rapid discontinuous rotations present a higher risk for the severe TBI than rapid discontinuous translations, and (2) that we cannot separately analyze rapid brain's rotations from translations, as they are in reality coupled.

Appendix: the $SE(3)$-group

Special Euclidean group $SE(3) := SO(3) \rhd \mathbb{R}^3$, (the semi-direct product of the group of rotations with the corresponding group of translations), is the Lie group consisting of isometries of the Euclidean 3D space $\mathbb{R}^3$.

An element of $SE(3)$ is a pair (A, a) where $A \in SO(3)$ and $a \in \mathbb{R}^3$. The action of $SE(3)$ on $\mathbb{R}^3$ is the rotation A followed by translation by the vector a and has the expression

$$(A, a) \cdot x = Ax + a.$$

The Lie algebra of the Euclidean group $SE(3)$ is $\mathfrak{se}(3) = \mathbb{R}^3 \times \mathbb{R}^3$ with the Lie bracket

$$[(\xi, u), (\eta, v)] = (\xi \times \eta, \xi \times v - \eta \times u). \qquad (10)$$

Using homogeneous coordinates, we can represent $SE(3)$ as follows,

---

[12] One practical application of the proposed model is in design of helmets. Briefly, a 'hard' helmet saves the skull but not the brain; alternatively, a 'soft' helmet protects the brain from the collision jolt but does not protect the skull. A good helmet is both 'hard' and 'soft'. In other words, if a human head covered with a solid helmet collides with a massive external body, the skull will be protected by the helmet—but the brain will still be shocked by the SE(3)-jolt, and a TBI will be caused. With or without the 'hard' helmet, brain's inertia tensor will be moved and rotated by the external SE(3)-jolt, and this will cause a brain injury, proportional to the jolt-collision with the head. Therefore, while protecting the skull is a necessary condition for protecting the brain, it is not enough. Brain's inertia tensor needs another kind of protection from the external collision-jolt. Contrastingly, if a human head covered with a 'soft' helmet collides with a massive external body, the helmet will dissipate the energy from the collision jolt, but will not necessarily protect the skull. As a result, a proper helmet would have to have both a hard external shell (to protect the skull) and a soft internal part (that will dissipate the energy from the collision jolt by its own destruction, in the same way as a car saves its passengers from the collision jolt by its own destruction). Note that, hypothetically speaking, an ideal shock-absorber is not a classical spring-damper system (with the distance-dependent spring and velocity-dependent damper), but rather a *constant-resistance damper*.

$$SE(3) = \left\{ \begin{pmatrix} R & p \\ 0 & 1 \end{pmatrix} \in GL(4, \mathbb{R}) : R \in SO(3), p \in \mathbb{R}^3 \right\},$$

with the action on $\mathbb{R}^3$ given by the usual matrix–vector product when we identify $\mathbb{R}^3$ with the section $\mathbb{R}^3 \times \{1\} \subset \mathbb{R}^4$. In particular, given

$$g = \begin{pmatrix} R & p \\ 0 & 1 \end{pmatrix} \in SE(3),$$

and $q \in \mathbb{R}^3$, we have

$$g \cdot q = Rq + p,$$

or as a matrix–vector product,

$$\begin{pmatrix} R & p \\ 0 & 1 \end{pmatrix} \begin{pmatrix} q \\ 1 \end{pmatrix} = \begin{pmatrix} Rq + p \\ 1 \end{pmatrix}.$$

The Lie algebra of $SE(3)$, denoted $\mathfrak{se}(3)$, is given by

$$\mathfrak{se}(3) = \left\{ \begin{pmatrix} \omega & v \\ 0 & 0 \end{pmatrix} \in M_4(\mathbb{R}) : \omega \in \mathfrak{so}(3), v \in \mathbb{R}^3 \right\},$$

where the attitude (or, angular velocity) matrix $\omega : \mathbb{R}^3 \to \mathfrak{so}(3)$ is given by

$$\omega = \begin{pmatrix} 0 & -\omega_z & \omega_y \\ \omega_z & 0 & -\omega_x \\ -\omega_y & \omega_x & 0 \end{pmatrix}.$$

The *exponential map*, $\exp : \mathfrak{se}(3) \to SE(3)$, is given by

$$\exp \begin{pmatrix} \omega & v \\ 0 & 0 \end{pmatrix} = \begin{pmatrix} \exp(\omega) & Av \\ 0 & 1 \end{pmatrix},$$

where

$$A = I + \frac{1 - \cos\|\omega\|}{\|\omega\|^2} \omega + \frac{\|\omega\| - \sin\|\omega\|}{\|\omega\|^3} \omega^2,$$

and $\exp(\omega)$ is given by the *Rodriguez' formula*,

$$\exp(\omega) = I + \frac{\sin\|\omega\|}{\|\omega\|} \omega + \frac{1 - \cos\|\omega\|}{\|\omega\|^2} \omega^2.$$

References

Bayly PV, Cohen TS, Leister EP, Ajo D, Leuthardt EC, Genin GM (2005) Deformation of the human brain induced by mild acceleration. J Neurotrauma 22(8):845–856

Beckwith JG, Chu JJ, Greenwald RM (2007) Validation of a noninvasive system for measuring head acceleration for use during boxing competition. J Appl Biomech 23(3):238–244

Bilby BA, Eshelby JD (1968) Dislocation and the theory of fracture. In: Liebowitz H (ed) Fracture, an advanced treatise. I, microscopic and macroscopic fundamentals. Academic Press, New York, London, pp 99–182

Bledsoe GH, Li G, Levy F (2005) Injury risk in professional boxing. South Med J 98(10):994–998

Brands DW, Peters GW, Bovendeerd PH (2004) Design and numerical implementation of a 3D non-linear viscoelastic

constitutive model for brain tissue during impact. J Biomech 37(1):127–134

Chen Z, Cao J, Cao Y, Zhang Y, Gu F, Zhu G, Hong Z, Wang B, Cichocki A (2008) An empirical EEG analysis in brain death diagnosis for adults. Cogn Neurodyn 2:257–271

Chu CS, Lin MS, Huang HM, Lee MC (1994) Finite element analysis of cerebral contusion. J Biomech 27(2):187–194

Cosserat E, Cosserat F (1898) Sur les equations de la theorie de l'elasticite. C R Acad Sci Paris 126:1089–1091

Cosserat E, Cosserat F (1909) Theorie des Corps Deformables. Hermann et Fils, Paris

Edelen DGB (1980) A four-dimensional formulation of defect dynamics and some of its consequences. Int J Eng Sci 18:1095

Eringen AC (2002) Nonlocal continuum field theories. Springer, New York

Goldsmith W (2001) The state of head injury biomechanics: past, present and future, part 1. Crit Rev Biomed Eng 29(5/6):441–600

Goldsmith W, Monson KL (2005) The state of head injury biomechanics: past, present, and future, part 2: physical experimentation. Crit Rev Biomed Eng 33(2):105–207

Guan Y, Zhang J, Yoganandan N, Pintar FA, Muszynski CA, Gennarelli TA (2006) Automating 3D meshing method for patient-specific modeling. Biomed Sci Instrum 42:199–204

Gutierrez E, Huang Y, Haglid K, Bao F, Hansson HA, Hamberger A, Viano D (2001) A new model for diffuse brain injury by rotational acceleration: I model, gross appearance, and astrocytosis. J Neurotrauma 18(3):247–257

Hoge CW, McGurk D, Thomas DL, Cox AL, Engel CC, Castro CA (2008) Mild traumatic brain injury in U.S. soldiers returning from Iraq. N Engl J Med 358(5):453–463

Hrapko M, van Dommelen JA, Peters GW, Wismans JS (2006) The mechanical behaviour of brain tissue: large strain response and constitutive modelling. Biorheology 43(5):623–636

Huang HM, Lee MC, Lee SY, Chiu WT, Pan LC, Chen CT (2000) Finite element analysis of brain contusion: an indirect impact study. Med Biol Eng Comput 38(3):253–259

Ivancevic V (2004) Symplectic rotational geometry in human biomechanics. SIAM Rev 46(3):455–474

Ivancevic V (2006) Lie-Lagrangian model for realistic human biodynamics. Int J Hum Rob 3(2):205–218

Ivancevic V, Aidman E (2007) Life-space foam: a medium for motivational and cognitive dynamics. Physica A 382:616–630

Ivancevic V, Ivancevic T (2006a) Natural biodynamics. World Scientific, Singapore

Ivancevic V, Ivancevic T (2006b) Human-like biomechanics. Springer, Dordrecht

Ivancevic V, Ivancevic T (2006c) Geometrical dynamics of complex systems: a unified modelling approach to physics, control, biomechanics, neurodynamics and psycho-socio-economical dynamics. Springer, Dordrecht

Ivancevic V, Ivancevic T (2007a) Neuro-fuzzy associative machinery for comprehensive brain and cognition modelling. Springer, Berlin

Ivancevic V, Ivancevic T (2007b) High-dimensional chaotic and attractor systems. Springer, Dordrecht

Ivancevic V, Ivancevic T (2007c) Computational mind: a complex dynamics perspective. Springer, Berlin

Ivancevic V, Ivancevic T (2007d) Complex dynamics: advanced system dynamics in complex variables. Springer, Dordrecht

Ivancevic V, Ivancevic T (2007e) Applied differential geometry: a modern introduction. World Scientific, Singapore

Ivancevic V, Ivancevic T (2008) Complex nonlinearity: chaos, phase transitions, topology change and path integrals. Springer, Berlin

Jian G, Xiao-ling L (1995) A physical theory of asymmetric plasticity. Appl Math Mech (Springer) 16(5):493–506

Kadic A, Edelen DGB (1983) A Gauge theory of dislocations and disclinations. Springer, New York

Krabbel G, Appel H (1995) Development of a finite element model of the human skull. J Neurotrauma 12(4):735–742

LaPlaca MC, Cullen DK, McLoughlin JJ, Cargill RS (2005) High rate shear strain of three-dimensional neural cell cultures: a new in vitro traumatic brain injury model. J Biomech 38(5):1093–1105

Lakes RS (1985) A pathological situation in micropolar elasticity. J Appl Mech 52:234–235

Lamb H (1932) Hydrodynamics (6th ed). Dover, New York

Leonard NE (1997) Stability of a bottom-heavy underwater vehicle. Automatica 33(3):331–346

Li J, Zhang J, Yoganandan N, Pintar F, Gennarelli T (2007) Regional brain strains and role of falx in lateral impact-induced head rotational acceleration. Biomed Sci Instrum 43:24–29

Loth F, Yardimci MA, Alperin N (2001) Hydrodynamic modelling of cerebrospinal fluid motion within the spinal cavity. J Biomech Eng 123(1):71–79

Maier SE, Hardy CJ, Jolesz FA (1994) Brain and cerebrospinal fluid motion: real-time quantification with M_mode MR imaging. Radiology 193(2):477–483

Mao H, Zhang L, Yang KH, King AI (2006) Application of a finite element model of the brain to study traumatic brain injury mechanisms in the rat. Stapp Car Crash J 50:583–600

Mason M (2007) Iraq war's signature wound: brain injury. Discover Magazine (February 23)

Mindlin RD (1965) Stress functions for a Cosserat continuum. Int J Solids Struct 1:265–271

Misra JC, Chakravarty S (1984) A study on rotational brain injury. J Biomech 17:459–466

Misra JC, Chakravarty S (1985) Dynamic response of a head–neck system to an impulsive load. Math Model 6:83–96

Morrison B, Cater HL, Benham CD, Sundstrom LE (2006) An in vitro model of traumatic brain injury utilising two-dimensional stretch of organotypic hippocampal slice cultures. J Neurosci Methods 150(2):192–201

NIH (2002) Traumatic brain injury: hope through research. NIH Publication No. 02-2478. National Institute of Health

Newman JA, Beusenberg MC, Shewchenko N, Withnall C, Fournier E (2005) Verification of biomechanical methods employed in a comprehensive study of mild traumatic brain injury and the effectiveness of American football helmets. J Biomech 38(7):1469–1481

Park J, Chung W-K (2005) Geometric integration on Euclidean group with application to articulated multibody systems. IEEE Trans Rob 21(5):850–863

Park HC, Lakes RS (1986) Cosserat micromechanics of human bone: strain redistribution by a hydration-sensitive constituent. J Biomech 19:385–397

Pena A, Pickard JD, Stiller D, Harris NG, Schuhmann MU (2005) Brain tissue biomechanics in cortical contusion injury: a finite element analysis. Acta Neurochir Suppl 95:333–336

Rapp PE (2008) Quantitative characterization of animal behavior following blast exposure. Cogn Neurodyn 1:287–293

Roth S, Raul JS, Ludes B, Willinger R (2007) Finite element analysis of impact and shaking inflicted to a child. Int J Legal Med 121(3):223–228

Runnerstam M, Bao F, Huang Y, Shi J, Gutierrez E, Hamberger A, Hansson HA, Viano D, Haglid K (2001) A new model for diffuse brain injury by rotational acceleration: II. Effects on extracellular glutamate, intracranial pressure, and neuronal apoptosis. J Neurotrauma 18(3):259–273

Sabet AA, Christoforou E, Zatlin B, Genin GM, Bayly PV (2008) Deformation of the human brain induced by mild angular head acceleration. J Biomech 41(2):307–315

Singh A, Lu Y, Chen C, Kallakuri S, Cavanaugh JM (2006) A new model of traumatic axonal injury to determine the effects of strain and displacement rates. Stapp Car Crash J 50:601–623

Sokoloff L (2008) The physiological and biochemical bases of functional brain imaging. Cogn Neurodyn 2:1–5

Takahashi T, Kato K, Ishikawa R, Watanabe T, Kubo M, Uzuka, T, Fujii Y, Takahashi H (2007) 3-D finite element analysis and experimental study on brain injury mechanism. In: Proceedings of the 29th annual international conference of the IEEE EMBS, Cité Internationale, Lyon, France, 23–26 August 2007

Viano DC, Casson IR, Pellman EJ, Bir CA, Zhang L, Sherman DC, Boitano MA (2005) Concussion in professional football: comparison with boxing head impacts—part 10. Neurosurgery 57(6):1154–1172

Viano DC, Casson IR, Pellman EJ (2007) Concussion in professional football: biomechanics of the struck player—part 14. Neurosurgery 61(2):313–327

Voo K, Kumaresan S, Pintar FA, Yoganandan N, Sances A Jr (2006) Finite-element models of the human head. Med Biol Eng Comput 34(5):375–381

Wolfson DR, McNally DS, Clifford MJ, Vloeberghs M (2005) Rigid-body modelling of shaken baby syndrome. Proc Inst Mech Eng 219(1):63–70

Yang JFC, Lakes RS (1981) Transient study of couple stress in compact bone: torsion. J Biomech Eng 103:275–279

Yang JFC, Lakes RS (1982) Experimental study of micropolar and couple-stress elasticity in bone in bending. J Biomech 15:91–98

Yang W, Tang J-C, Ing Y-S, Ma C-C (2001) Transient dislocation emission from a crack tip. J Mech Phys Solids 49(10):2431–2453

Yoganandan N, Pintar FA, Zhang J, Stemper BD, Philippens M (2008) Upper neck forces and moments and cranial angular accelerations in lateral impact. Ann Biomed Eng 36(3):406–414

Zhang L, Yang KH, King AI (2001) Comparison of brain responses between frontal and lateral impacts by finite element modeling. J Neurotrauma 18(1):21–30

Zhang L, Yang KH, King AI (2004) A proposed injury threshold for mild traumatic brain injury. J Biomech Eng 126(2):226–236

Zhang J, Yoganandan N, Pintar FA, Gennarelli TA (2006) Role of translational and rotational accelerations on brain strain in lateral head impact. Biomed Sci Instrum 42:501–506

Zong Z, Lee HP, Lu C (2006) A three-dimensional human head finite element model and power flow in a human head subject to impact loading. J Biomech 39(2):284–292

Zou H, Schmiedeler JP, Hardy WN (2007) Separating brain motion into rigid body displacement and deformation under low-severity impacts. J Biomech 40(6):1183–1191